nature structural & molecular biology

Structure of a KirBac potassium channel with an open bundle crossing indicates a mechanism of channel gating

Vassiliy N Bavro[1,6,7], Rita De Zorzi[2,7], Matthias R Schmidt[1,3], João R C Muniz[4], Lejla Zubcevic[1], Mark S P Sansom[3,5], Catherine Vénien-Bryan[2,5,6] & Stephen J Tucker[1,5]

KirBac channels are prokaryotic homologs of mammalian inwardly rectifying (Kir) potassium channels, and recent crystal structures of both Kir and KirBac channels have provided major insight into their unique structural architecture. However, all of the available structures are closed at the helix bundle crossing, and therefore the structural mechanisms that control opening of their primary activation gate remain unknown. In this study, we engineered the inner pore-lining helix (TM2) of KirBac3.1 to trap the bundle crossing in an apparently open conformation and determined the crystal structure of this mutant channel to 3.05 Å resolution. Contrary to previous speculation, this new structure suggests a mechanistic model in which rotational 'twist' of the cytoplasmic domain is coupled to opening of the bundle-crossing gate through a network of inter- and intrasubunit interactions that involve the TM2 C-linker, slide helix, G-loop and the CD loop.

Inwardly rectifying potassium (Kir) channels regulate membrane electrical excitability and K^+ transport in a wide range of cell types. Their activity controls many diverse processes such as heart rate, vascular tone, insulin secretion and salt and fluid balance, and an increasing number of disease states are now known to be directly associated with abnormal Kir channel function[1]. Like many other types of ion channels, the activity of Kir channels is controlled by dynamic conformational changes that regulate the flow of K^+ ions through the central pore of the channel[1,2]. This process is known as 'gating', and understanding the molecular mechanism of these dynamic changes in Kir channel structure is critical to our understanding of how these channels function in both health and disease.

The primary gating mechanism in most classes of K^+ channel is thought to involve an iris-like motion of the pore-lining inner transmembrane helices that constrict the permeation pathway at the helix bundle crossing[3]. In voltage-gated K^+ channels, this gating motion is physically coupled to the movement of a transmembrane voltage sensor, whereas in Kir channels, conformational changes within the large cytoplasmic domains (CTD) are thought to control movement of the bundle-crossing gate[3–6]. This provides a mechanism for the action of ligands such as G-proteins, ATP, H^+ and PIP_2, which all bind to these intracellular domains to regulate Kir channel function[1,2]. Other structural domains, such as the selectivity filter and the cytoplasmic G-loop, have also been proposed to act as physical gates in Kir channels[7–10]. However, their role is secondary to that of the bundle-crossing gate, which is regarded as the primary activation gate in all major classes of K^+ channels and which must always be in an open conformation for the channel to be conductive.

Full understanding of these gating processes requires high-resolution structural information of a Kir channel trapped in multiple gating conformations, and over the last few years, several different Kir channel structures have been solved by X-ray crystallography; these include a eukaryotic Kir channel[11], a number of homologous prokaryotic KirBac channels[4] and the chimeras between them[12], and a series of structures of KirBac3.1 with the CTD in multiple orientations[13]. However, in all of these Kir and KirBac channel structures, the bundle-crossing gate is closed, and despite their enormous value, they therefore provide limited insight into the structural changes that must occur to allow these channels to open. This apparent preference for the bundle-crossing gate to crystallize in the closed state strongly suggests that it must represent a low-energy state of the channel and that new strategies are therefore required to stabilize the open state of the channel.

In this study we now report the X-ray crystal structure of an open-state KirBac channel at 3.05 Å resolution. This structure not only illustrates how the bundle crossing opens but, more importantly, suggests how opening of the primary activation gate may be physically coupled to conformational changes in the CTD.

RESULTS

Overall structure of a mutant KirBac3.1 channel

We previously isolated a number of mutations in KirBac3.1 that directly increase channel activity[14]. Many of these mutations

[1]Clarendon Laboratory, Department of Physics, University of Oxford, Oxford, UK. [2]Laboratory of Molecular Biophysics, Department of Biochemistry, University of Oxford, Oxford, UK. [3]Structural Bioinformatics and Computational Biochemistry Unit, Department of Biochemistry, University of Oxford, Oxford, UK. [4]Structural Genomics Consortium, University of Oxford, Oxford, UK. [5]OXION Ion Channel Initiative, University of Oxford, Oxford, UK. [6]Present Address: School of Immunity and Infection, University of Birmingham, Birmingham UK (V.N.B.); Institut de Minéralogie et de Physique des Milieux Condensés, Université Pierre et Marie Curie, Centre National de la Recherche Scientifique, UMR 7590, Paris, France (C.V.-B.). [7]These authors contributed equally to this work. Correspondence should be addressed to C.V.-B. (catherine.venien@impmc.upmc.fr) or S.J.T. (stephen.tucker@physics.ox.ac.uk).

Received 11 July 2011; accepted 14 November 2011; published online 8 January 2012; doi:10.1038/nsmb.2208

Table 1 Data collection and refinement statistics

	KirBac3.1(S129R)
Data collection	
Space group	$P42_12$
Cell dimensions	
a = *b*, *c* (Å)	106.24, 89.80
Resolution (Å)	106.24–3.05 (3.21–3.05)[a]
R_{merge}	0.262 (0.945)
$I / \sigma I$	5.5 (2.0)
Completeness (%)	99.9 (99.8)
Redundancy	6.8 (6.9)
Refinement	
Resolution (Å)	89.80–3.05
No. reflections	10,244
R_{work} / R_{free} (%)	22.04 / 25.89
No. atoms	2,218
Protein	2,191
Ligand/ion	7
Water	20
B-factors	54.39
Protein	54.67
Ligand/ion	40.77
Water	29.34
R.m.s. deviations	
Bond lengths (Å)	0.010
Bond angles (°)	1.08

[a]Values in parentheses are for the highest-resolution shell.

introduced charged amino acids into TM2, suggesting that the steric or charge repulsion between these side chains may assist channel opening at the bundle crossing. We therefore reasoned that such mutants might have the ability to stabilize the open state of the channel. One such gating mutant is S129R, which is located very close to the bundle crossing, and in most other Kir or KirBac channels, this residue is a glycine[15,16].

We previously expressed and purified this mutant channel and showed that it is functionally active[14]. In the present study, we therefore crystallized this mutant and grew crystals belonging to the $P42_12$ space group, which were diffracted up to 3.05 Å resolution. The structure was solved by molecular replacement, and a final model containing 280 out of 301 residues of the construct was refined to an *R*-factor of 22.0% and an R_{free} of 25.9%, with 99.6% of the residues in the final model lying in the most favorable and additionally allowed regions of the Ramachandran plot. The full data collection and refinement statistics are shown in **Table 1**. Visualization of this structure and comparison to KirBac3.1 in the closed state revealed major structural changes in the transmembrane helices and also at the bundle crossing (**Fig. 1a**,**b**).

KirBac3.1 trapped in an apparently open conformation

In all of the previous KirBac3.1 structures, the bundle-crossing gates are fully closed[13]. This is defined by a tight constriction of the pore at Tyr132 in TM2, which occludes the conductive pathway and acts as the gate at this position[2,4,17]. However, in the structure presented here, the S129R mutation has trapped the bundle crossing in an apparently open conformation (**Fig. 1**). In the closed-state structures of KirBac3.1, the Cα–Cα distances at Tyr132 range from 12.2 Å to 13.5 Å (ref. 13), whereas in the S129R mutant, this distance is increased to 17.1 Å (**Fig. 1b**). The engineered mutant Arg129 side chains in TM2 create an additional constriction within the pore (**Supplementary Fig. 1**). However, because Arg129 is a serine in wild-type KirBac3.1 and a glycine in all other Kir or KirBac channels[18,19], we therefore analyzed the pore radius of this new structure with a serine at position 129. This reveals that the bundle-crossing gate would be open and conductive when the channel is in this conformation and that there is free access to the selectivity filter from the intracellular side of the channel (**Fig. 1c**,**d**). The S129R mutation therefore appears to have stabilized the TM helices and the bundle-crossing gate in a conformation that mimics the wild-type channel in an open state.

Bending of TM2 at the glycine hinge

The global rearrangements propagating from these changes at the bundle crossing are in agreement with earlier modeling studies of TM2 motions in KirBac3.1 (ref. 20) as well as the gating motions

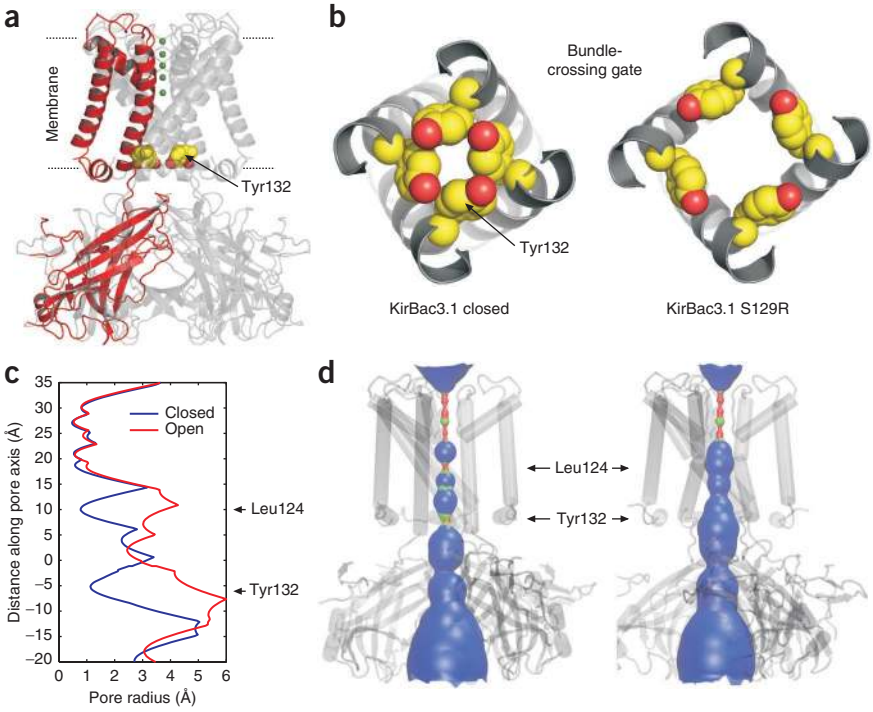

Figure 1 Structure of the KirBac3.1 S129R mutant in an apparently open conformation. (**a**) Overall structure of S129R mutant with one subunit highlighted in red for clarity. Ions within the selectivity filter are shown in green, and residue Tyr132, which forms the primary gate at the bundle crossing, is shown as CPK spheres in all four subunits. (**b**) Bottom-up view of the bundle-crossing gate in an example of a closed-state KirBac3.1 (PDB 2WLJ)[13] and the S129R mutant channel. Tyr132 side chains are shown as CPK spheres. (**c**) Pore-radius profile of a closed-state KirBac3.1 (PDB 2WLJ) (closed, blue) and the S129R mutant, in which the Arg129 side chain has been replaced by a serine (open, red). (**d**) The pore-lining surface and structure of the open and closed KirBac3.1 channels, with the position of the major constrictions Tyr132 and Leu124 marked by arrows.

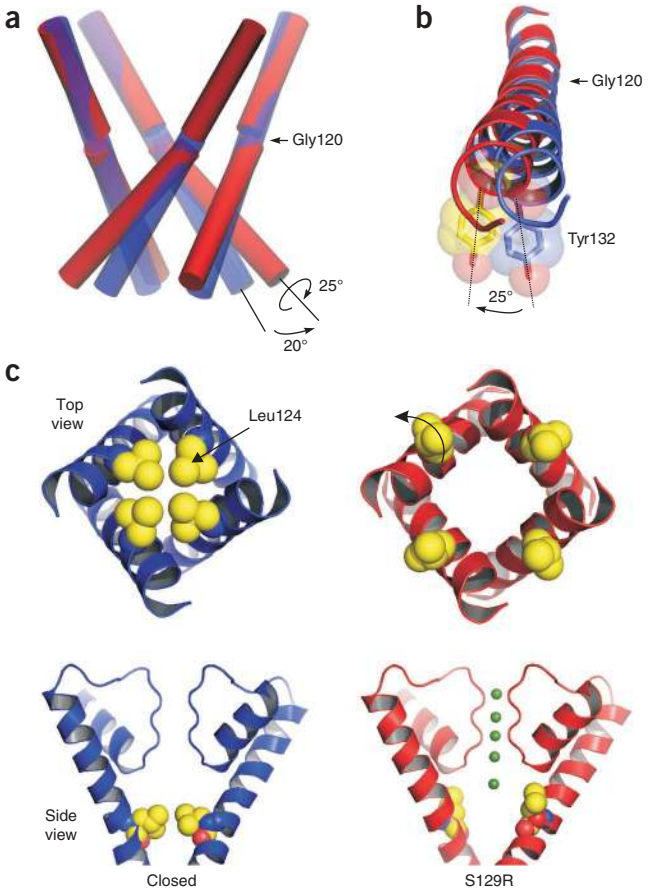

Figure 2 Bending of the inner TM2 helices during channel opening. (**a**) Conformational changes of the inner helices from the closed state (blue cylinders) to the conformation (red cylinders) seen in the S129R mutant. The lower section of TM2 kinks by up to 20° at the conserved glycine hinge (Gly120) and also rotates around its helical axis by 25° when viewed from below. (**b**) The clockwise rotation of TM2 is shown viewed from below. Overlay of TM2 helices from the S129R structure (red) and a closed-state Kir3.1 (blue, PDB 2WLJ). Tyr132 is shown as a transparent CPK sphere. (**c**) Opening of the inner cavity constriction formed by Leu124. Top and side views are shown on the S129R structure and a closed state KirBac3.1 (PDB 2WLJ). The position of ions within the filter of the S129R structure is shown in green. The rotation of TM2 moves Leu124 away from the pore. Leu124 is equivalent to the rectification control site in the TM2 of eukaryotic Kir channels.

observed in the open-state crystal structures of truncated and full-length KcsA[21–23]. Compared to the closed state, the lower part of TM2 bends by up to 20° at a highly conserved glycine hinge residue[18,19] (Gly120 in KirBac3.1), whereas the upper part remains relatively rigid. However, in addition to this bending or kinking of TM2, we also observe a rotation or twisting of the lower section of TM2 along its helical axis by approximately 25° (**Fig. 2a**,**b**), and there is good overlay of the TM2 helices of KirBac3.1 S129R with the open 17-Å crystal structure of KcsA (**Supplementary Fig. 2**)[21,22]. No twisting is observed in the outer helix (TM1) during opening of the bundle crossing; however, TM1 is displaced outward and follows the movement of TM2 (see **Supplementary Movie 1**).

Rotation of TM2 opens a secondary gate within the pore

This rotational movement of TM2 is important, because in addition to the bundle-crossing gate (Tyr132), a secondary constriction exists at Leu124 in the closed-state structures (**Fig. 1c**)[13,17]. Rotation of TM2 induced by opening of the bundle crossing means that Leu124 is now twisted away from the central cavity, thus increasing the effective pore diameter at this position from less than 2 Å to >8 Å (**Fig. 2c**). Poisson-Boltzmann electrostatic calculations reveal a marked reduction in the energetic barrier to K^+ permeation at this point (**Supplementary Fig. 3**), producing an electrostatic profile that becomes progressively more favorable for the movement of K^+ toward the selectivity filter in this open conformation. Movement of this side chain upon channel opening is also particularly noteworthy, because Leu124 in KirBac3.1 is equivalent to the TM2 rectification control site in eukaryotic Kir channels (for example, Asp172 in Kir2.1)[24].

A twisted yet conductive conformation of KirBac3.1

In a recently reported series of KirBac3.1 structures[13], the CTD shows considerable rotational diversity with respect to the pore, that is, the twist and non-twist conformations. Comparison of these structures to the S129R structure shows that it is rotated and in a twist configuration (**Fig. 3a**). It was also suggested that the twist or non-twist status

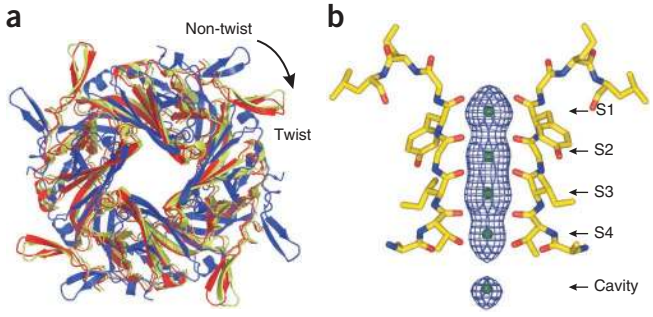

of the different closed-state structures correlates with the conductive status of the selectivity filter, with only the non-twist conformations being conductive[13]. However, despite being in the twist conformation, analysis of the ion occupancy in the S129R structure shows that all four K^+ binding sites (S1–S4) are occupied (**Fig. 3b**), which is clearly representative of a conductive filter conformation[21,22,25,26]. This new conformation is therefore in direct contrast to the gating model recently proposed[13].

The C-linker couples pore opening to movement of the CTD

A common mechanistic theme in other major classes of tetrameric cation channels is that allosteric changes in domains attached to the TM helices are mechanically coupled to opening and closing of the bundle crossing gate[3]. A rotational movement or twist of the CTD could therefore conceivably promote opening of the bundle-crossing gate[4,13]. However, this would require tight physical coupling of the TM helices to the CTD. Therefore, in this new structure, it is noteworthy that the C-linker between TM2 and the CTD is displaced relative to its position in the non-twist conformation (**Fig. 4a**). This causes the C-linker to become involved in a network of interactions that links the bundle-crossing gate with the slide helix as well as with the two

Figure 3 KirBac3.1 S129R is in a twisted yet conductive conformation. (**a**) The CTD of a non-twist (blue, PDB 2WLJ) and twist (yellow, PDB 2X6C) conformation[13] are viewed from the top relative to their superimposed pore domains (not shown). The relative position of the S129R CTD is also overlaid (red), showing that it is in the twist conformation. (**b**) $F_o - F_c$ omit map of electron density in the selectivity filter of the S129R mutant channels contoured at ~3σ, showing clear density in all four binding sites as well as the cavity site.

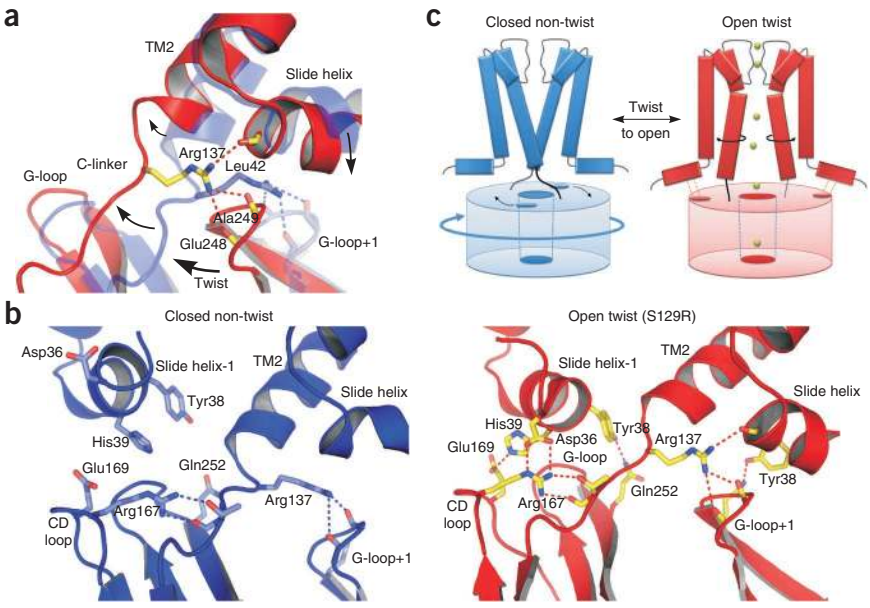

Figure 4 Interaction network between the CTD and the TMD. (**a**) The C-linker in the twist S129R structure (red) is displaced by up to 5 Å compared to the closed non-twist structure (PDB 2WLJ, transparent blue). During twisting and opening, Arg137 shifts its interaction with backbone carbonyls on the G-loop of the adjacent subunit (G-loop+1) to include an intrasubunit interaction with the slide helix. The major motions are indicated by arrows. (**b**) Comparison of the network of interactions formed in the S129R twist open conformation with those in a closed non-twist conformation (PDB 2WLJ). Movement of the slide helix and displacement of the C-linker allow an extensive network of inter- and intrasubunit interactions to form (see also **Supplementary Movie 2**). (**c**) Cartoon of gating model proposed by the motions observed in the S129R structure. The twist conformation of the CTD prepares the C-linker and also brings the slide helix into register with the CD loop (dot shown on CTD), thereby coupling rotational movement of the CTD to opening of the bundle-crossing gate.

loops within the CTD (the CD loop and the G-loop) that have been implicated in the control of channel gating[7,12,27,28]. These interactions would stabilize the interface between the twisted CTD and the TM pore domain (TMD) in the open state (**Fig. 4b**).

One of the residues in this network is the highly conserved Arg137 within the C-linker itself, which provides a direct interaction between the C-linker and the G-loop of the adjacent subunit. A similar interaction is observed in some of the closed-state structures[13], but local rearrangements caused by opening of the bundle crossing now displace the C-linker, allowing Arg137 to form an additional intrasubunit contact with a backbone carbonyl of Leu42 on the slide helix (**Fig. 4a**).

This network is further expanded by interaction of the C-linker with a highly conserved arginine on the CD loop of the CTD (Arg167), thereby providing an additional connection to the slide helix of the adjacent subunit (**Fig. 4b**). This connection can only occur in the twist conformations, because when it is compared to the non-twist structures (**Fig. 4b**), there is a downward movement of the slide helix, bringing Asp36 into direct contact with both the η- and ε-nitrogens of Arg167 on the CD loop of the adjacent subunit. This also brings His39 into contact with Glu169 (**Fig. 4b** and **Supplementary Fig. 4**). Movement of the slide helix and its interaction with the CD loop is seen in other twisted structures[13], but in this new conformation, this extended network is now directly coupled to the opening of the bundle-crossing gate.

Other previously unknown interactions also form upon opening of the bundle-crossing gate. Notably, the highly conserved Tyr38 in the slide helix now interacts with Gln252 in the G-loop (**Fig. 4b**), and disruption of this interaction (with mutation Y38F) reduces the functional activity of KirBac3.1, consistent with its possible role in stabilization of the open state (**Supplementary Fig. 5**). Also notably, unlike the Asp36-Arg167 interaction, which takes place on the outer surface of the slide helix, the Tyr38-Gln252 interaction occurs on the inner side of the slide helix and results in a direct intersubunit linkage between the slide helix of one subunit and both the CD- and G-loops of the adjacent subunit.

DISCUSSION

In this study we present the first high-resolution structure of a KirBac channel with the bundle-crossing gate in an open conformation. This new structure provides a substantial extension to the conformational landscape available for this class of dynamic proteins; it demonstrates that TM2 bends at a conserved glycine hinge and that rotation of TM2 also contributes to opening of a secondary gate within the pore. Furthermore, opening of the bundle-crossing gate involves a network of interactions between the TMD and CTD that illustrate how rotational movement of the CTD may be coupled to channel gating.

It has been suggested that the selectivity filter has an important role in Kir or KirBac channel gating, and indeed, several of our recent studies, including X-ray footprinting of KirBac3.1 as well as the identification of gating mutations, directly support this notion[14,29]. However, the filter can only act as a gate if and when the bundle crossing is open, and until now high-resolution structural information about how the primary activation gate opens has been unavailable. Engineering the bundle-crossing gate of KirBac3.1 into a conformation that mimics the open state has therefore allowed us, for the first time, to visualize a potential mechanism of channel opening.

The major structural changes that occur in TM2 as the bundle-crossing gate opens are consistent with those seen in other open state K^+ channels, and a similar rotation of TM2 has recently been observed in the open-state structure of full-length KcsA[23]. Importantly, this rotation of TM2 also opens a secondary gate within the inner cavity of KirBac3.1 at Leu124. Although Leu124 will not act as a gate independently of the bundle crossing, it may have an important role in sealing the pore in the closed state, as it is located just below the cavity ion binding site (**Fig. 2c**). Notably, movement of Leu124 was also detected by our previous X-ray footprinting study of KirBac3.1 (ref. 29), and a similar rotation of the equivalent residue in KcsA (Phe103) has recently been observed[23]. However, of perhaps greater importance is the fact that Leu124 is equivalent to the rectification control site in TM2 of eukaryotic Kir channels (for example, Asp172 in Kir2.1 (ref. 24)), where the presence of a negatively charged side chain influences the binding of Mg^{2+} and polyamines and thereby influences the degree of inward rectification. Rotational movement of this side chain during channel opening (**Fig. 2**) could therefore have a major role in defining how these classical pore blockers interact with this site in the open versus the closed states.

Whether this KirBac3.1 structure represents a fully open conformation is not known. Much wider openings of the bundle crossing

(up to 32 Å) have been observed with truncated versions of KcsA[21,22]. However, the presence of the C-terminal domain in KcsA appears to restrict these openings to about 21 Å (ref. 23), and so the large KirBac CTD is also likely to impose structural constraints on the size of the maximal opening that can occur. Nevertheless, the S129R mutant is functionally active, therefore a wider dilation must be possible to overcome the artificial constriction formed by the mutant Arg129 side chains (**Supplementary Fig. 1**). Notably, introduction of a negative charge at position 129 also activates KirBac3.1 (**Supplementary Fig. 5**), and similarly charged mutations at the bundle crossing have been shown to activate both KirBac and Kir channels[14,30], suggesting that wider openings must be possible in these mutant channels.

It has previously been suggested that the rotational status of the CTD is directly linked to the conductive state of the selectivity filter and that this does not require movement of the bundle-crossing gate. In particular, it was proposed that the twist configuration induces a nonconductive selectivity filter[13]. However, the new structure we present here is in the twist configuration, yet it is both conductive within the filter and open at the bundle crossing, thus directly contradicting the gating model proposed previously[13]. At this stage, it is not yet known whether any functional form of C-type inactivation occurs within the selectivity filter of KirBac3.1, but it is likely that any allosteric coupling between the TM helices and the selectivity filter will require a movement of the bundle-crossing gate similar to that seen in the elegant crystallographic studies of KcsA[21–23,31].

Instead, this new conformation suggests a model in which rotational movement of the CTD may be directly coupled to channel opening at the bundle-crossing gate, and that the twist configuration is a prerequisite for this to occur. Similarly, although it has been proposed that the G-loop acts as an independent gate[7,12], and it is clearly an important regulator of Kir or KirBac channel activity[8], its primary role may be to couple conformational changes in the CTD to the C-linker and thereby to opening of the bundle-crossing gate.

Importantly, this mechanism also provides a rationale for the action of a number of compounds that are likely to influence these interactions—for example, cholesterol with the CD loop[28] and PIP_2 with the C-linker and CTD[32,33]. In particular, we find it interesting that in eukaryotic Kir channels, which are activated by PIP_2, the C-linker contains an insertion of three additional charged residues (**Supplementary Fig. 6**) thought to interact with PIP_2 and that would clearly influence this gating mechanism when they are present[34]. In support of this idea, a structure of chicken Kir2.2 has very recently been solved with PIP_2 bound, and although this structure is also closed at the bundle crossing, it appears to represent a 'pre-open' state where PIP_2 interacts directly with the C-linker to create tension in this region in preparation for opening of the bundle crossing[35]. Given the fundamentally conserved structural basis of K^+ channel gating at the bundle crossing, it is perhaps not unexpected that the C-linker appears to have such an important role in Kir or KirBac channel gating and is consistent with similar roles for this linker region in the gating of other tetrameric cation channels[36–39].

In conclusion, the gating model suggested by this new conformation is markedly different from that proposed previously[13]. Instead of being an obstacle to channel opening, we propose that the twist configuration is required in order for the bundle-crossing gate to open, by allowing a network of interactions to form between the TMD and CTD, and we present a simplified cartoon model summarizing how this is done (**Fig. 4c** and **Supplementary Movie 2**). Clearly, further work will be required to determine the causality of the changes we observed in the structure of the bundle-crossing gate and the network of newly discovered interactions that this produces. Similarly, the question of whether the bundle crossing opens wider than the 17-Å opening seen here will also be the subject of future studies. Nevertheless, this new open-state structure of KirBac3.1 now provides an important extension to the available conformational landscape for this important class of ion channels.

METHODS

Methods and any associated references are available in the online version of the paper at http://www.nature.com/nsmb/.

Accession codes. The atomic coordinates of the KirBac3.1 S129R structure have been deposited in the Protein Data Bank under the accession code 3ZRS.

Note: Supplementary information is available on the Nature Structural & Molecular Biology website.

ACKNOWLEDGMENTS

We thank the staff at the I24 beamline at the Diamond Light Source. This work was supported by the Biotechnology and Biological Sciences Research Council and the Wellcome Trust. R. DeZ was supported by a Marie Curie Intra-European Fellowship.

AUTHOR CONTRIBUTIONS

S.J.T. and C.V.-B. conceived and designed the research. R. De Z. and V.N.B. expressed and crystallized the mutant protein. V.N.B., R. De Z. and L.Z. collected the diffraction data. V.N.B. and J.R.C.M. determined and refined the structure with contribution from R. De Z., V.N.B., L.Z. and M.R.S. analyzed and interpreted the structure. L.Z. conducted complementation studies. C.V.-B., M.S.P.S. and S.J.T. supervised the project. V.N.B. and S.J.T. wrote the manuscript with the help of comments from all authors.

COMPETING FINANCIAL INTERESTS

The authors declare no competing financial interests.

Published online at http://www.nature.com/nsmb/.
Reprints and permissions information is available online at http://www.nature.com/reprints/index.html.

1. Hibino, H. *et al.* Inwardly rectifying potassium channels: their structure, function, and physiological roles. *Physiol. Rev.* **90**, 291–366 (2010).
2. Bichet, D., Haass, F.A. & Jan, L.Y. Merging functional studies with structures of inward-rectifier K^+ channels. *Nat. Rev. Neurosci.* **4**, 957–967 (2003).
3. Swartz, K.J. Towards a structural view of gating in potassium channels. *Nat. Rev. Neurosci.* **5**, 905–916 (2004).
4. Kuo, A. *et al.* Crystal structure of the potassium channel KirBac1.1 in the closed state. *Science* **300**, 1922–1926 (2003).
5. Kuo, A., Domene, C., Johnson, L.N., Doyle, D.A. & Venien-Bryan, C. Two different conformational states of the KirBac3.1 potassium channel revealed by electron crystallography. *Structure* **13**, 1463–1472 (2005).
6. Domene, C., Doyle, D.A. & Venien-Bryan, C. Modeling of an ion channel in its open conformation. *Biophys J.* **89**, L01–L03 (2005).
7. Pegan, S. *et al.* Cytoplasmic domain structures of Kir2.1 and Kir3.1 show sites for modulating gating and rectification. *Nat. Neurosci.* **8**, 279–287 (2005).
8. Proks, P. *et al.* A gating mutation at the internal mouth of the Kir6.2 pore is associated with DEND syndrome. *EMBO Rep.* **6**, 470–475 (2005).
9. Proks, P., Antcliff, J.F. & Ashcroft, F.M. The ligand-sensitive gate of a potassium channel lies close to the selectivity filter. *EMBO Rep.* **4**, 70–75 (2003).
10. Domene, C., Klein, M.L., Branduardi, D., Gervasio, F.L. & Parrinello, M. Conformational changes and gating at the selectivity filter of potassium channels. *J. Am. Chem. Soc.* **130**, 9474–9480 (2008).
11. Tao, X., Avalos, J.L., Chen, J. & MacKinnon, R. Crystal structure of the eukaryotic strong inward-rectifier K^+ channel Kir2.2 at 3.1 A resolution. *Science* **326**, 1668–1674 (2009).
12. Nishida, M., Cadene, M., Chait, B.T. & Mackinnon, R. Crystal structure of a Kir3.1-prokaryotic Kir channel chimera. *EMBO J.* **26**, 4005–4015 (2007).
13. Clarke, O.B. *et al.* Domain reorientation and rotation of an intracellular assembly regulate conduction in Kir potassium channels. *Cell* **141**, 1018–1029 (2010).
14. Paynter, J.J. *et al.* Functional complementation and genetic deletion studies of KirBac channels: activatory mutations highlight gating-sensitive domains. *J. Biol. Chem.* **285**, 40754–40761 (2010).
15. Sun, S., Gan, J.H., Paynter, J.J. & Tucker, S.J. Cloning and functional characterization of a superfamily of microbial inwardly rectifying potassium channels. *Physiol. Genomics* **26**, 1–7 (2006).

16. Shang, L. & Tucker, S.J. Non-equivalent role of TM2 gating hinges in heteromeric Kir4.1/Kir5.1 potassium channels. *Eur. Biophys. J.* **37**, 165–171 (2008).
17. Tai, K., Haider, S., Grottesi, A. & Sansom, M.S. Ion channel gates: comparative analysis of energy barriers. *Eur. Biophys. J.* **38**, 347–354 (2009).
18. Magidovich, E. & Yifrach, O. Conserved gating hinge in ligand- and voltage-dependent K+ channels. *Biochemistry* **43**, 13242–13247 (2004).
19. Jin, T. *et al.* The βγ subunits of G proteins gate a K^+ channel by pivoted bending of a transmembrane segment. *Mol. Cell* **10**, 469–481 (2002).
20. Grottesi, A., Domene, C., Hall, B. & Sansom, M.S. Conformational dynamics of M2 helices in KirBac channels: helix flexibility in relation to gating via molecular dynamics simulations. *Biochemistry* **44**, 14586–14594 (2005).
21. Cuello, L.G. *et al.* Structural basis for the coupling between activation and inactivation gates in K^+ channels. *Nature* **466**, 272–275 (2010).
22. Cuello, L.G., Jogini, V., Cortes, D.M. & Perozo, E. Structural mechanism of C-type inactivation in K^+ channels. *Nature* **466**, 203–208 (2010).
23. Uysal, S. *et al.* Mechanism of activation gating in the full-length KcsA K^+ channel. *Proc. Natl. Acad. Sci. USA* **108**, 11896–11899 (2011).
24. Stanfield, P.R. *et al.* A single aspartate residue is involved in both intrinsic gating and blockage by Mg^{2+} of the inward rectifier, IRK1. *J. Physiol. (Lond.)* **478**, 1–6 (1994).
25. Zhou, Y., Morais-Cabral, J.H., Kaufman, A. & MacKinnon, R. Chemistry of ion coordination and hydration revealed by a K^+ channel-Fab complex at 2.0 Å resolution. *Nature* **414**, 43–48 (2001).
26. Bernèche, S. & Roux, B. Energetics of ion conduction through the K^+ channel. *Nature* **414**, 73–77 (2001).
27. Singh, D.K., Rosenhouse-Dantsker, A., Nichols, C.G., Enkvetchakul, D. & Levitan, I. Direct regulation of prokaryotic Kir channel by cholesterol. *J. Biol. Chem.* **284**, 30727–30736 (2009).
28. Rosenhouse-Dantsker, A., Leal-Pinto, E., Logothetis, D.E. & Levitan, I. Comparative analysis of cholesterol sensitivity of Kir channels: role of the CD loop. *Channels (Austin)* **4**, 63–66 (2010).
29. Gupta, S. *et al.* Conformational changes during the gating of a potassium channel revealed by structural mass spectrometry. *Structure* **18**, 839–846 (2010).
30. Khurana, A. *et al.* Forced gating motions by a substituted titratable side chain at the bundle crossing of a potassium channel. *J. Biol. Chem.* **286**, 36686–36693 (2011).
31. Cordero-Morales, J.F. *et al.* Molecular determinants of gating at the potassium-channel selectivity filter. *Nat. Struct. Mol. Biol.* **13**, 311–318 (2006).
32. D'Avanzo, N., Cheng, W.W., Wang, S., Enkvetchakul, D. & Nichols, C.G. Lipids driving protein structure? Evolutionary adaptations in Kir channels. *Channels (Austin)* **4**, 139–141 (2010).
33. Tucker, S.J. & Baukrowitz, T. How highly charged anionic lipids bind and regulate ion channels. *J. Gen. Physiol.* **131**, 431–438 (2008).
34. Leal-Pinto, E. *et al.* Gating of a G protein-sensitive mammalian Kir3.1 prokaryotic Kir channel chimera in planar lipid bilayers. *J. Biol. Chem.* **285**, 39790–39800 (2010).
35. Hansen, S.B., Tao, X. & MacKinnon, R. Structural basis of PIP_2 activation of the classical inward rectifier K^+ channel Kir2.2. *Nature* **477**, 495–498 (2011).
36. Taraska, J.W. & Zagotta, W.N. Structural dynamics in the gating ring of cyclic nucleotide-gated ion channels. *Nat. Struct. Mol. Biol.* **14**, 854–860 (2007).
37. Schumacher, M.A., Rivard, A.F., Bachinger, H.P. & Adelman, J.P. Structure of the gating domain of a Ca^{2+}-activated K^+ channel complexed with Ca^{2+}/calmodulin. *Nature* **410**, 1120–1124 (2001).
38. Long, S.B., Campbell, E.B. & Mackinnon, R. Voltage sensor of Kv1.2: structural basis of electromechanical coupling. *Science* **309**, 903–908 (2005).
39. Enkvetchakul, D., Jeliazkova, I., Bhattacharyya, J. & Nichols, C.G. Control of inward rectifier K channel activity by lipid tethering of cytoplasmic domains. *J. Gen. Physiol.* **130**, 329–334 (2007).

ONLINE METHODS

Protein expression and crystallization. The S129R mutant was introduced using site-directed mutagenesis into a synthetic KirBac3.1 in pET30a, where the open reading frame had been codon-optimized for expression in *Escherichia coli*. The protocol for expression and purification of this mutant channel was identical to that previously described for wild-type KirBac3.1 (ref. 29), and following gel filtration, the triDM detergent was exchanged into 14 mM HEGA-10 using Vivaspin concentrators with a 100-kDa cutoff. Protein crystals were then grown using the sitting-drop method in 10% (v/v) glycerol, 90 mM HEPES 7.2, 20% (v/v) PEG 400, 5% (w/v) PEG 4000 and 2.5% (w/v) PEG 8000, using ~6 mg ml^{-1} protein concentration in a 1:1 protein:reservoir ratio. Crystals appeared after 3–4 d at 20 °C and were cryocooled under liquid nitrogen before analysis.

Data collection and structure determination. The KirBac3.1 S129R crystals belong to the $P42_12$ space group, with cell dimensions of $a = b = 106.2$ Å and $c = 89.8$ Å. The asymmetric unit has a solvent content of 69.4% and contains one molecule. Data were collected at 100 K using a Pilatus 6M detector at the I-24 beamline at the Diamond Light Source, at a wavelength of $\lambda = 0.9778$ Å to a resolution of up to 3.05 Å. Data set statistics are provided in **Table 1**. Data were processed with Mosflm and Scala (CCP4 program)[40] and the space group confirmed with Pointless[41]. Five percent of the reflections were set aside in the free *R* set. Molecular replacement was carried out with Phaser (CCP4 suite)[42], using a search model derived from PDB 2X6C, processed with Chainsaw (CCP4)[40]. The model was refined in real space interactively using Coot[43] and refined using BUSTER-TNT[44], which included a final round of translation, libration and screw-rotation (TLS) anisotropic refinement, as implemented in BUSTER-TNT. The final model contains 280 residues out of 301 (residues 12–26, 33–277 and 281–300, inclusive); in addition, connectivity between residues 26 and 32 can be established at a lower sigma threshold, but they were not included in the final model, as it was not possible to build and refine residues in this region at full occupancy with certainty. The model also contains 20 solvent molecules and seven ions. Ions are positioned on the four-fold axis and are therefore modeled with occupancies of less than 25%. The final model was validated using MolProbity[45] and presented very good stereochemistry, with over 99.6% of all residues in favored and additionally allowed regions of the Ramachandran plot.

Structure analysis. The superimpositions of the individual domains were done using LSQKAB (CCP4-supported program) and analyzed in Coot[43]. The ribbon diagrams and actual videos were made with PyMOL (http://www.pymol.org/). Cavity analysis was carried out using HOLE[46], and cylinder representations and cavity visualizations were done with VMD[47]. The contribution to the electrostatic potential of a potassium ion along the pore axis of the channel was calculated using the Adaptive Poisson-Boltzmann Solver (APBS) package[48], with a methodology similar to the one previously applied to nanopores[49]. The potassium ion pathway and axis were defined using the program HOLE, which was also used to calculate pore radii. Charges and radii were assigned using PDB2PQR[50], which was also used to add missing atoms of unresolved side chains before calculating electrostatic energies. Energies were calculated using a NaCl bath with an ionic strength of 0.2 M at 298 K. The protein (dielectric constant $\varepsilon = 10$) was embedded into a dielectric slab ($\varepsilon = 2$), mimicking the membrane environment, with membrane thickness set to 45 Å. The pore itself was excluded from the membrane and assigned a solvent dielectric ($\varepsilon = 80$). Supplementary movies were animated using PyMOL. Starting structures were aligned along the transmembrane domain of 2WLJ (residues Trp46–Gly120) before interpolation. Intermediate structures were calculated using GROMACS4 (ref. 51). The consensus secondary structure was modeled after the secondary structure of 3ZRS. Missing extracellular loops in 2X6C and the missing βL-M loop in 3ZRS were built using MODELLER 9.9 (ref. 52).

40. Collaborative Computational Project, Number 4. The CCP4 suite: programs for protein crystallography. *Acta Crystallogr. D Biol. Crystallogr.* **50**, 760–763 (1994).
41. Evans, P. Scaling and assessment of data quality. *Acta Crystallogr. D Biol. Crystallogr.* **62**, 72–82 (2006).
42. McCoy, A.J. *et al.* Phaser crystallographic software. *J. Appl. Crystallogr.* **40**, 658–674 (2007).
43. Emsley, P., Lohkamp, B., Scott, W.G. & Cowtan, K. Features and development of Coot. *Acta Crystallogr. D Biol. Crystallogr.* **66**, 486–501 (2010).
44. Blanc, E. *et al.* Refinement of severely incomplete structures with maximum likelihood in BUSTER-TNT. *Acta Crystallogr. D Biol. Crystallogr.* **60**, 2210–2221 (2004).
45. Chen, V.B. *et al.* MolProbity: all-atom structure validation for macromolecular crystallography. *Acta Crystallogr. D Biol. Crystallogr.* **66**, 12–21 (2010).
46. Smart, O.S., Wang, X., Wallace, B.A. & Sansom, M.S. HOLE: a program for the analysis of the pore dimensions of ion channel structural models. *J. Mol. Graph.* **14**, 354–360, 376 (1996).
47. Humphrey, W., Dalke, A. & Schulten, K. VMD - Visual Molecular Dynamics. *J. Mol. Graph.* **14**, 33–38 (1996).
48. Holst, M.J. & Saied, F. Numerical solution of the nonlinear Poisson-Boltzmann equation: Developing more robust and efficient methods. *J. Comput. Chem.* **16**, 337–364 (1995).
49. Beckstein, O., Tai, K. & Sansom, M.S. Not ions alone: Barriers to ion permeation in nanopores and channels. *J. Am. Chem. Soc.* **126**, 14694–14695 (2004).
50. Dolinsky, T.J. *et al.* PDB2PQR: expanding and upgrading automated preparation of biomolecular structures for molecular simulations. *Nucleic Acids Res.* **35**, W522–W525 (2007).
51. Van Der Spoel, D. *et al.* GROMACS: Fast, flexible and free. *J. Comput. Chem.* **26**, 1701–1718 (2005).
52. Sali, A.A. & Blundell, T.L. Comparative protein modelling by satisfaction of spatial restraints. *J. Mol. Biol.* **234**, 779–815 (1993).

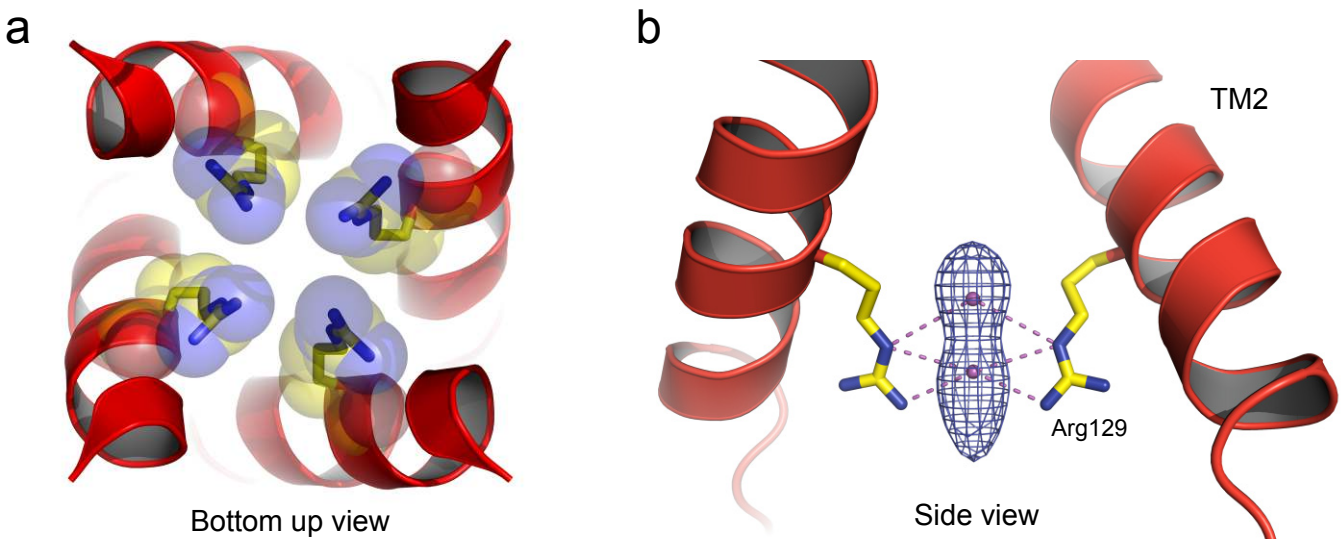

Supplementary Figure 1. Location of S129R mutation. **a**: Bottom up view of inner cavity showing the Arg129 side chains as sticks with transparent vdw spheres. The presence of the engineered mutant Arg129 side-chain creates an additional constriction point within the pore not present in wild-type KirBac3.1 where this residue is a serine, or in any other Kir/KirBac channel where this residue is normally a glycine. **b**: F_O-F_C OMIT map (blue mesh contoured at σ 2.7) in the vicinity of the engineered Arg129 mutation. The two apparent peaks in the density were modelled as chloride ions based upon APBS calculations and coordination geometry. In wild-type KirBac3.1 (Ser129) this engineered constriction would not be present.

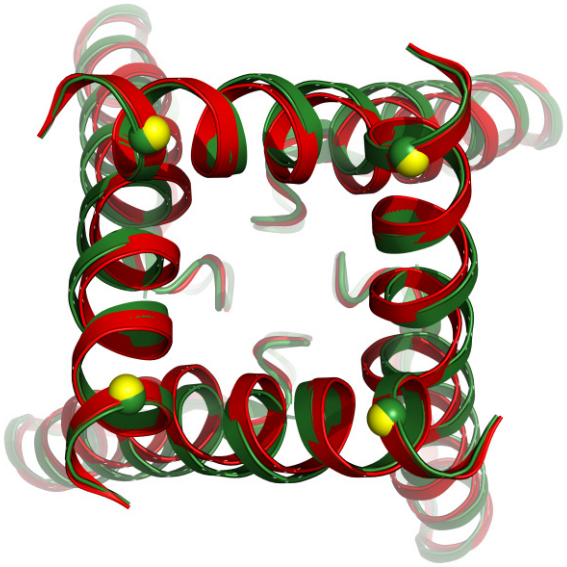

Supplementary Figure 2. Overlay of S129R opening with 17 Å open KcsA. Bottom-up view showing overlay of the TM2 helices of KirBac3.1(S129R) structure (in red) with those of the open 17 Å KcsA structure (PDB code 3F7Y) (shown in green). The bundle-crossing in the KcsA structure is 17.1 Å open at T112 (Cα atoms shown as green spheres) which matches well with the 17.2Å opening seen at the equivalent A133 residue in TM2 of the KirBac3.1 (S129R) structure (Cα atom shown as yellow spheres).

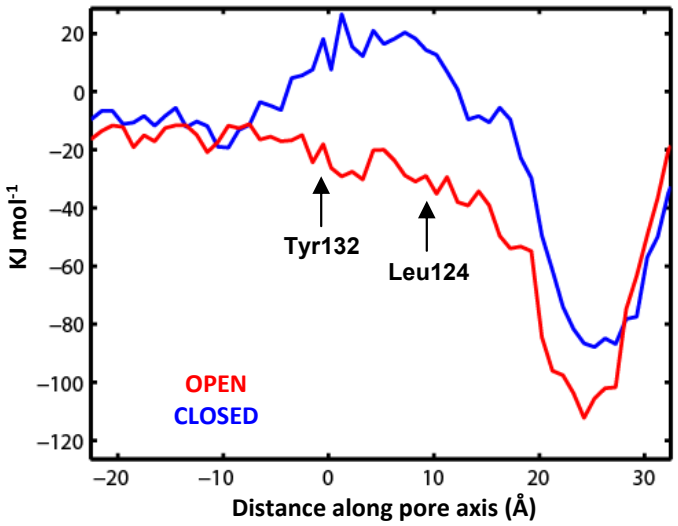

Supplementary Figure 3 Electrostatic energy profile of the open pore. The energy profile of a K^+ ion along the pore axis was calculated using APBS. Compared are an example of a closed wild-type KirBac3.1 channel (PDB code 2X6C shown in blue) compared to the open conformation found in the S129R mutant where the mutant Arg129 side chain is replaced by a serine as found in wild-type KirBac3.1. The position of the constrictions formed by Tyr132 at the bundle crossing and Leu124 within the inner cavity are marked. This indicates that the energetic barrier to permeation is removed in this novel open conformation and there is an increasingly favourable energetic gradient for movement of K^+ through the pore from the intracellular side towards the selectivity filter.

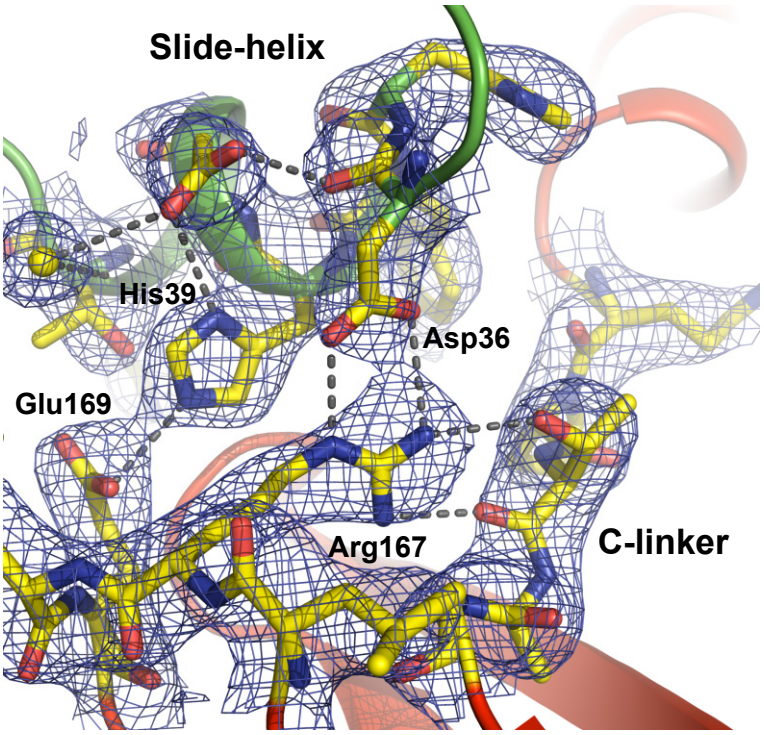

Supplementary Figure 4 Interaction between the slide-helix and CD-loop. The KirBac3.1(S129R) mutant structure is in the twist configuration where Asp36 and His39 on the slide helix interact with Arg167 and Glu169 on the slide-helix. However, displacement of the C-linker when the bundle-crossing is open creates an additional interaction between Arg167 and backbone carbonyls of the C-linker. This 2Fo-Fc electron density is contoured at 1.5σ above the mean (refined to 3.05Å). All the major features of these interactions at this interface are clearly discernable.

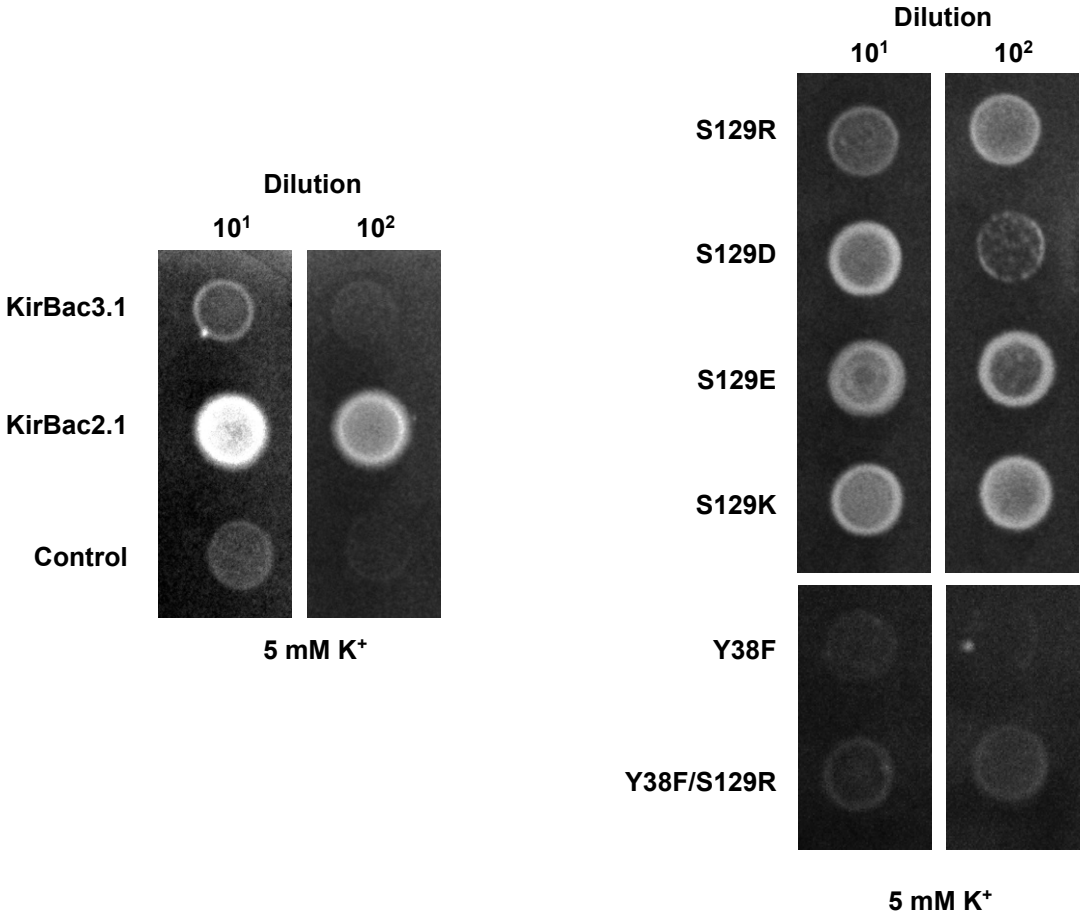

Supplementary Figure 5 Functional studies of KirBac3.1 mutants. Complementation of growth defect in K^+ uptake-deficient *E.coli* (TK2420) by introduction of charged residues at residue 129. Wild-type KirBac3.1 (Ser129) does not complement growth defect on 5mM [K^+] media. Control is pQE60 vector alone. Positive control for growth is KirBac2.1 (Ref.15). Mutation S129R was previously identified as an activatory mutation by random mutagenesis of WT KirBac3.1 and selection on low [K^+] media (Ref.14). Introduction of a negative charge by site-directed mutagenesis (Asp129 or Glu129) also increases channel activity, as does introduction of a positive charge (Arg129 or Lys129). S129A or S129L mutations do not complement growth (not shown). Disruption of the interaction network shown in Figure 4 with the Y38F mutation produces a reduction in channel activity in agreement with the gating model shown in Figure 4; the Y38F mutation by itself shows no activity (similar to WT KirBac3.1), but its effect can be seen in combination with the S129R mutation where it reduces the overall activity of the S129R mutation. Assays were performed as previously described (Ref.14).

```
   Kir1.1  ...MGASERS VFRVLIRALT ERMFKHLR.. .RWFITHIFG RSRQRARLVS   44
   Kir2.2  ...MTAGRVN PYSIVSSEED GLRLTTMPGI NGFGNGKIHT RRKCRNRFVK   47
KirBac1.1  .......... ........MN VDPFSPHS.. .....SDSFA QAASPARKPP   25
KirBac3.1  .......... .......... .......... ....MTGGMK PPARKPRILN   16

   Kir1.1  KEGR..CNIE FGNVDAQSRF IFFVDIWTTV LDLKWRYKMT VFITAFLGSW   92
   Kir2.2  KNGQ..CNVE FTNMDDKP.Q RYIADMFTTC VDIRWRYMLL LFSLAFLVSW   94
KirBac1.1  RGGRRIWSGT REVIAYGMPA SVWRDLYYWA LKVSWPVFFA SLAALFVVNN   75
KirBac3.1  SDGS..SNIT RLGLEKRG.. .WLDDHYHDL LTVSWPVFIT LITGLYLVTN   61

   Kir1.1  FLFGLLWYVV AYVHKDLPEF YPPDNRTPCV ENINGMTSAF LFSLETQVTI  142
   Kir2.2  LLFGLIFWLI ALIHGDLENP GGDDTFKPCV LQVNGFVAAF LFSIETQTTI  144
KirBac1.1  TLFALLYQLG DAPIANQS.. .........P PGFVG...AF FFSVETLATV  111
KirBac3.1  ALFALAYLAC GDVIENAR.. .......... PGSFTD..AF FFSVQTMATI   97

   Kir1.1  GYGFRFVTEQ CATAIFLLIF QSILGVIINS FMCGAILAKI SRPKKRAKTI  192
   Kir2.2  GYGFRCVTEE CPLAVFMVVV QSIVGCIIDS FMIGAIMAKM ARPKKRAQTL  194
KirBac1.1  GYGD..MHPQ TVYAHAIATL EIFVGMSGIA LSTGLVFARF ARP...RAKI  156
KirBac3.1  GYGK..LIPI GPLANTLVTL EALCGMLGLA VAASLIYARF TRP...TAGV  142

   Kir1.1  TFSKNAVISK RGGKLCLLIR VANLRKSLLI GSHIYGKLLK TTITPEGETI  242
   Kir2.2  LFSHNAVVAM RDGKLCLMWR VGNLRKSHIV EAHVRAQLIK PRITEEGEYI  244
KirBac1.1  MFARHAIVRP FNGRMTLMVR AANARQNVIA EARAKMRLMR REHSSEG.YS  205
KirBac3.1  LFSSRMVISD FEGKPTLMMR LANLRIEQII EADVHLVLVR SEISQEG.MV  191

   Kir1.1  ILDQTNINFV VDAGNENLFF ISPLTIYHII DHNSPFFHMA AETLSQQDFE  292
   Kir2.2  PLDQIDIDVG FDKGLDRIFL VSPITILHEI NEDSPLFGIS RQDLETDDFE  294
KirBac1.1  LMKIHDLKLV RNEHP...IF LLGWNMMHVI DESSPLFGET PESLAEGRAM  252
KirBac3.1  FRRFHDLTLT RSRSP...IF SLSWTVMHPI DHHSPIYGET DETLRNSHSE  238

   Kir1.1  LVVFLDGTVE STSATCQVRT SYVPEEVLWG YRFVPIVSKT KEGKYRVDFH  342
   Kir2.2  IVVILEGMVE ATAMTTQARS SYLASEILWG HRFEPVLFEE .KNQYKVDYS  343
KirBac1.1  LLVMIEGSDE TTAQVMQARH AWEHDDIRWH HRYVDLMSDV .DGMTHIDYT  301
KirBac3.1  FLVLFTGHHE AFAQNVHARH AYSCDEIIWG GHFVDVFTTL PDGRRALDLG  288

   Kir1.1  NFGKTVEVET PHCAMCLYN. .E..KDARAR MKRGYDNPNF VLSEVDETDD  388
   Kir2.2  HFHKTYEVPS TPRCSAKD.L VENKFLLPST NSFCYENELA FMSRDEDEED  392
KirBac1.1  RFNDTEPVEP PGAAPDAQ.. .....AFAAK PGEGDARPV. ..........  333
KirBac3.1  KFHEIAQ... .......... .......... .......... ..........  295
```

Supplementary Figure 6 Sequence Alignment. KirBac3.1 is aligned with the sequences of KirBac1.1, Kir1.1 and chicken Kir2.2. Those residues in KirBac3.1 which form part of the stabilization network shown in Figure 4 are highlighted in red, whilst the two residues which form the major constrictions within the pore of the closed state KirBac3.1 (Leu124 and Tyr132) are shown in blue. TM1 and TM2 are underlined. Eukaryotic Kir channels contain an insertion of 3 charged residues in the C-linker (in bold).